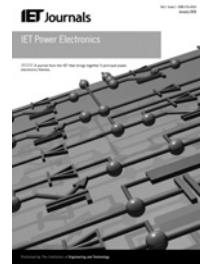


Published in IET Power Electronics
 Received on 2nd July 2013
 Revised on 15th January 2014
 Accepted on 26th February 2014
 doi: 10.1049/iet-pel.2013.0511



ISSN 1755-4535

Design and implementation of a high-frequency LC-based half-bridge resonant converter for dielectric barrier discharge ozone generator

Muhammad Amjad^{1,2}, Zainal Salam¹

¹Centre for Electrical Energy Systems, Faculty of Electrical Engineering, Universiti Teknologi Malaysia, 81310 Johor Bahru, Johor, Malaysia

²University College of Engineering and Technology, The Islamia University of Bahawalpur, 63100, Bahawalpur, Pakistan
 E-mail: zainals@fke.utm.my

Abstract: This study describes the design and implementation of a high-frequency resonant converter based on the transformerless half-bridge inverter topology. The transformer can be omitted because the voltage gain of the 'LC' tank circuit (without transformer) is sufficiently high to overcome the initiation voltage and to maintain steady ozone yield. Another important contribution of the work is the increase in operating frequencies, that is, up to 95 kHz. This increase has two main benefits: (i) smaller resonant component values (which lead to a smaller size of converter) and (ii) lower initiation voltage. To validate the theory, the high-frequency power converter is designed and tested on a dielectric barrier discharge chamber. It is shown that ozone yield is improved and the ozone formation starts at lower chamber voltages. The experimental and simulation results are found to be in close agreement and hence to validate the design procedures.

1 Introduction

Nowadays, ozone gas (O₃) has been widely recognised as a very effective oxidising agent and has been used in a wide range of applications. It leaves no harmful residues to the environment and is a safer alternative to other oxidants such as chlorine, peroxide and dichromate [1]. The most effective and economical method to generate ozone in a normal atmospheric environment is by using an electrical microdischarges method – such as corona, pulsed and dielectric barrier discharge (DBD). The latter is preferred because of the creation of non-equilibrium plasma at atmospheric pressure [2].

The DBD chamber is constructed using two electrodes and a dielectric layer that covers at least one of the electrodes. The purpose of the dielectric is to distribute the microdischarges evenly over the entire electrode surface. The most common material for dielectric is ceramic and glass. The space between the electrodes is known as the discharge gap, where air/oxygen is converted into ozone by applying high voltage across it. If glass or ceramic is used as dielectric, the potential required to initiate the discharge (known as the initiation voltage) is about 10–20 kV for a 1–2 mm discharge gap [3].

Conventionally, a line frequency (50/60 Hz) power supply is used to power up the ozone generator. This consists of a variac and high-voltage transformer that is coupled to the ozone chamber [4]. Despite its simplicity, the line frequency generator is bulky and inefficient. A more preferable approach is to utilise high-frequency power supplies. They are known to be more efficient, and can

produce higher ozone yield at a lower applied voltage. Among the typical topologies are the full-bridge, push-pull and class E resonant inverters. Examples of important work related to full-bridge ozone power supply are presented by Koudriavtsev *et al.* [5] and Kinnares and Hothongkham [6]. In [6], the topology consists of a rectifier and a series compensating inductor placed at the primary. The circuit is operated at 57.5 kHz, and the voltage is stepped up using a high-frequency transformer. In [5], the inductor is placed at the secondary with an operating frequency of 7 kHz. An ozone generator based on a push-pull inverter operating at 5 kHz is implemented in [7–9]. The topology requires two additional inductors, which are placed at the primary of the transformer and are used as chokes. In [10–12], class E, the single-switch resonant inverter operating at 15 kHz is presented.

In all the aforementioned converters, high-frequency ferrite transformers are used to obtain high voltage across the ozone chamber. Although it is much smaller (because of the smaller core and much fewer turns), the transformer exhibits several drawbacks, namely: (i) the occurrence of high voltage and current spike in the switches because of leakage inductances [12, 13], (ii) low efficiency and (iii) it is the source of electromagnetic interference. Moreover, the requirement for additional inductors increases the cost and reduces the efficiency of the power converter. To overcome these problems, the piezoelectric transformer (PT) has been introduced by Alonso *et al.* [13–15] as an alternative to ferrite. The work proposes a highly efficient PT-based ozone power supply, operated at 40.6 kHz. Despite its promising prospect, the control of PT is more complicated

because of its narrow resonant bandwidth, which mandates a closed-loop operation. Moreover, high-power PTs are not readily available in the market; hence, the power supply can deliver very limited power (<10 W). Another approach is to use transformerless topology, as proposed by Amjad *et al.* [16]. In their work, the ‘LCL’ resonant power converter is designed at 33.5 kHz. However, the removal of the transformer requires two additional large inductors to ensure that the required initiation voltage is achieved.

Apart from the applied voltage, a higher operational frequency of the power supply is recognised as one of the possible factors to increase the ozone yield. To date, the typical frequency range is 7–60 kHz; the highest is being demonstrated by Kinnares and Hothongkham [6], at 57.5 kHz. It would be interesting to develop an ozone power that can operate at higher than the typical frequencies and to discover what are the design issues, constraints and problems. Another important consideration is cost and performance trade-off. The simplest topology is the single-switch resonant converter. Although, it needs only one switch, it requires a large choke (in tens of mH) connected in series with a DC source to regulate the input current [17, 18]. Furthermore, its performance is inferior to other resonant topologies [12]. On the other hand, the full-bridge is preferable because of its higher efficiency and the ability to handle larger power. However, it utilises four switches and each switch requires a gate drive circuit and its associated protection circuit. This increases the cost and size of the power converter.

In view of these factors, this work proposes a high-frequency half-bridge transformerless power converter for ozone generation. The half-bridge is selected because it requires only two switches, but it exhibits performance that matches the full-bridge circuit. The transformer can be omitted because the voltage gain of the ‘LC’ tank circuit (without transformer) is sufficiently high to overcome the initiation voltage and to maintain steady ozone yield. Unlike other topology, the use of the inductor as choke is not necessary [19]. Another major contribution of this work is the increase in operating frequencies, that is, up to 95 kHz. Consequently, the resonant circuit values will be low, which allows the reduction of the converter size.

The remainder of the paper is structured as follows. Section 2 presents the high-frequency characterisation of the ozone chamber. In Section 3, the proposed topology and its circuit operation are outlined. The design of resonant circuit values is described in Section 4. Experimental results are provided in Section 5. The conclusions are drawn in Section 6 of the paper.

2 Ozone chamber parameter determination

In this work, the DBD chamber is constructed in a rectangular planar shape, as depicted in Fig. 1. The idea is to simplify the

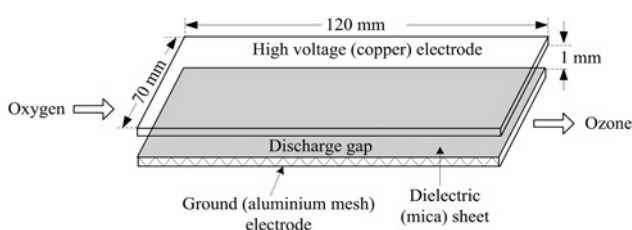


Fig. 1 Planar DBD chamber configuration

construction and to achieve modularity in design. The chamber consists of a pair of electrodes, a discharge gap and a dielectric layer that covers one of the electrodes. To produce ozone at lower voltage, material with minimum thickness is the most essential factor [20]. Muscovite mica has been chosen primarily because it is available in thin sheet, that is, <0.1 mm. Despite its thinness, mica is flexible and non-breakable. This characteristic is preferable to glass, which is fragile and can be easily broken when made into very thin sheet. The dimension of each electrode is 120 mm × 70 mm. The discharge gap is designed to be 1 mm. The high-voltage electrode is made of plane copper material. For higher ozone production, aluminium mesh is selected as the ground electrode to create a non-uniform electric field [21]. The mesh electrode is constructed from aluminium mesh wires with square patterns with dimensions of 1.5 mm × 1.5 mm.

An ozone chamber behaves similar to a capacitor, because it is made from two parallel electrodes and separated by dielectric and discharge gap. The chamber can be considered as a connection of two capacitors in series: (i) the capacitance because of the discharge gap (C_a) and (ii) the capacitance because of the dielectric sheet (C_d). Effectively C_a and C_d can be represented by a single capacitance (C_g). The power supplied to the ozone chamber is represented by the power dissipated in R_g . Thus, the linear model of an ozone chamber at high frequency is represented by a parallel combination of C_g and R_g [22].

The chamber parameters, that is, C_g and R_g are calculated using the resonance technique, as suggested in [23]. The experimental setup to find the parameters consists of a DC power supply, full-bridge inverter, gate drive circuit and a known value inductor (L_s) as depicted in Fig. 2. The parallel-loaded circuit is created by connecting the L_s with the ozone chamber. The input to the parallel-loaded circuit is a square waveform; consequently, the voltage and current waveform at resonance is sinusoidal. The chamber parameters C_g and R_g are calculated using the following equations

$$C_g = \frac{1}{(2\pi f_r)^2 L_s} \quad (1)$$

$$R_g = A_v(2\pi f_r)L_s \quad (2)$$

Using the frequency sweep method, the switching frequency of the inverter is varied slowly by the gate drive circuit until the voltage and current waveforms are maximum and sinusoidal. With $L_s = 20$ mH and $V_{in} = 30$ V, the voltage and current waveform of the ozone chamber are as illustrated in

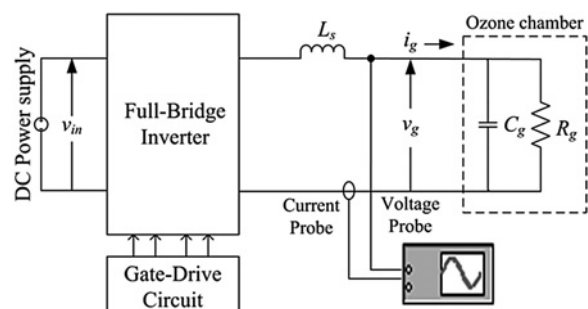


Fig. 2 Experimental setup for chamber parameter determination

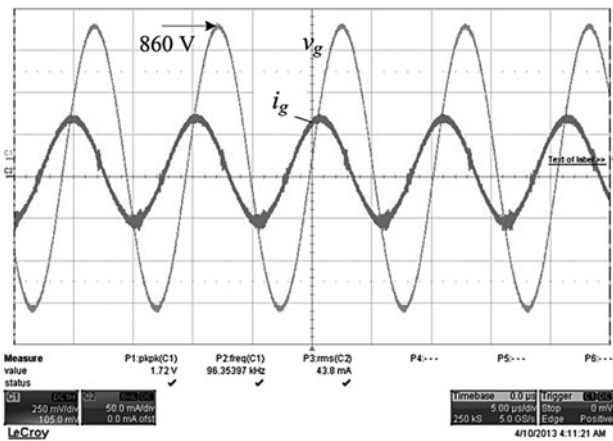


Fig. 3 Ozone chamber voltage and current waveform at resonant frequency of 96.3 kHz

Fig. 3. The resonant frequency (f_r) and voltage gain (A_v) obtained experimentally are 96.3 kHz and 22.3, respectively. Using (1) and (2), C_g and R_g are computed to be 136.6 pF and 270 k Ω , respectively.

3 Proposed ozone generation system

3.1 Experimental setup

The proposed ozone generation system using a $L_s C_p$ resonant circuit is shown in Fig. 4. It consists of a high-frequency pulse width modulated (PWM) half-bridge inverter, a resonant tank and an ozone chamber. In the half-bridge inverter, the metal-oxide semiconductor field-effect transistors (MOSFETs) M_1 and M_2 are switched in anti-phase to provide a quasi-square wave input to the $L_s C_p$ resonant circuit. For the power switches, the IRFP 460 MOSFETs equipped with freewheeling diodes are selected. The gate drive circuit consists of PWM LM3524D and HCPL-3120 integrated circuits (ICs). The PWM IC outputs are taken from emitters of two NPN transistors, which are driven 180° out of phase. Moreover, the gate drive circuit is designed to provide a stable AC sweep frequency up to 300 kHz. Each PWM output is used to drive the HCPL-3120 optocouplers that provide the gating signal for the MOSFETs of the inverter.

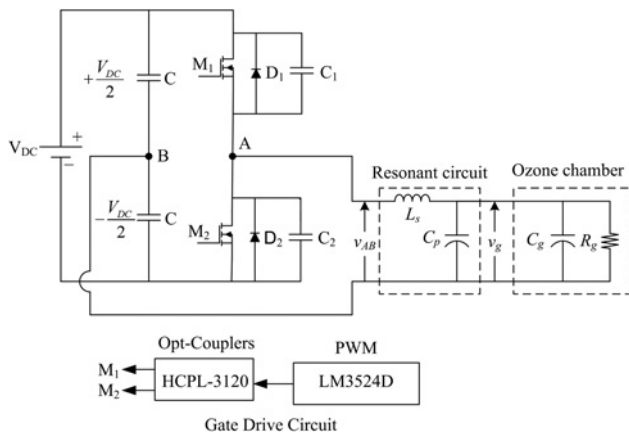


Fig. 4 Proposed ozone generation system

3.2 Circuit operation

The switching pattern of the half-bridge switches, voltage and current waveforms of each element of the inverter are shown in Fig. 5. For zero-voltage zero-current switching operation, a duty factor of 25% is employed between the switching. This is known as class DE inverter control [24]. Moreover, the operating frequency of the inverter is selected to be above the resonant frequency. If the inverter is operated above the resonant frequency of the circuit, the input current will lag the input voltage (v_{AB}). Note that the resonant of the circuit is the combination of $L_s C_p$ with the chamber capacitance, that is, C_g . The phase lag of current and duty factor between the switches are adjusted until each switch turns on when current is current and zero voltage across it. The circuit operation, which corresponds to the switching pattern, can be divided into four modes. Their timing diagrams are illustrated in Fig. 6.

Mode 1 ($t_0 - t_1$): This is also known as the rectifying mode. The switch M_1 turns ON and the DC source supplies energy to the 'RLC' load (which is the combination of the 'LC' resonant circuit and ozone chamber). The input voltage (V_{AB}) to the load is $+V_{DC}/2$ and current flows from

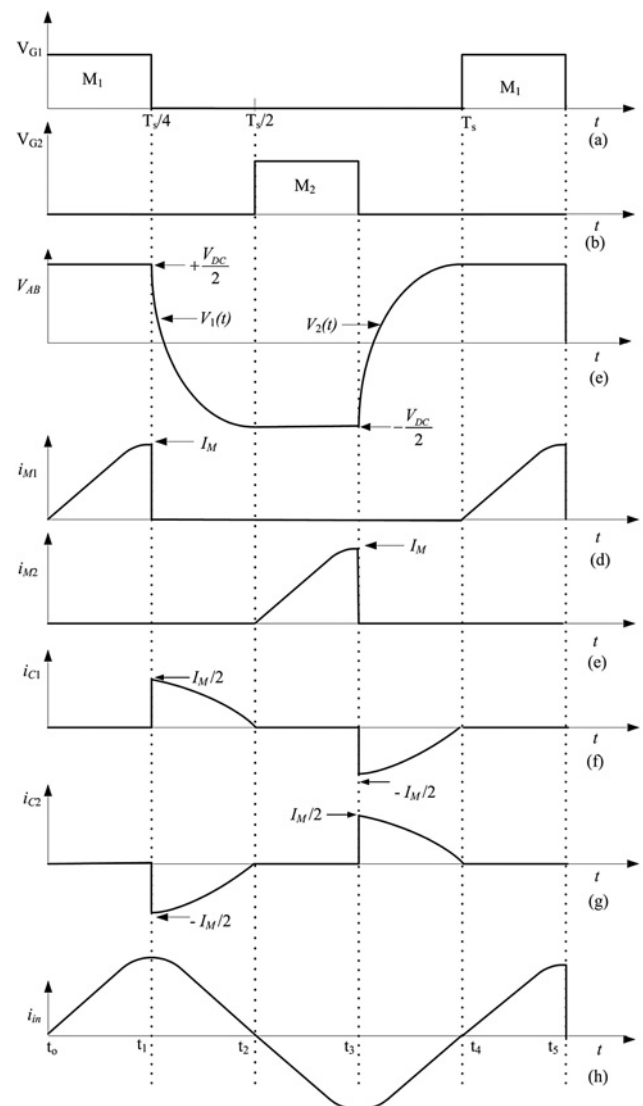


Fig. 5 Operational waveforms of half-bridge inverter

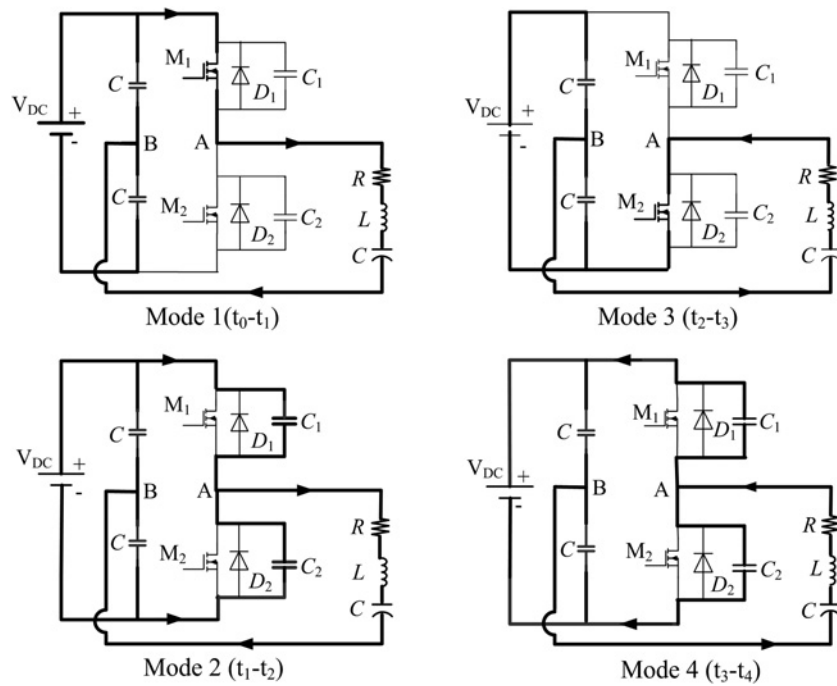


Fig. 6 Operating modes of half-bridge inverter

the DC source to the load via M_1 . The voltage across M_1 and C_1 is zero, whereas the voltage across M_2 and C_2 is $+V_{DC}$. The current flowing through M_1 is given by

$$i_{M1} = I_m \sin \omega t \quad (3)$$

Mode 2 ($t_1 - t_2$): During this interval, both the switches turn OFF. The current flows to charge C_1 from 0 to $+V_{DC}/2$. Hence

$$i_{C1} = \frac{I_m}{2} \sin \omega t \quad (4)$$

Moreover, the load current discharges C_2 from $+V_{DC}/2$ to 0 can be written as

$$i_{C1} = -\frac{I_m}{2} \sin \omega t \quad (5)$$

Mode 3 ($t_2 - t_3$): M_2 turns ON and the DC power supply provides energy to the load. This mode is also called the rectifying mode. The current flows from the DC power supply to the load via switch M_2 and the voltage V_{AB} is $-V_{DC}/2$. The voltages across M_1 , C_1 and D_1 are $+V_{DC}$ and the voltages across M_2 , C_2 and D_2 are zero. The current flowing through M_2 is given by

$$i_{M2} = I_m \sin \omega t \quad (6)$$

Mode 4 ($t_3 - t_4$): During this mode all the switches are turned OFF. The load current is diverted from M_2 to charge C_2 from 0 to $V_{DC}/2$ and is given by

$$i_{C2} = \frac{I_m}{2} \sin \omega t \quad (7)$$

The load current discharges C_1 from $V_{DC}/2$ to 0 to provide zero-voltage switching (ZVS) for M_1 and is given by

$$i_{C1} = -\frac{I_m}{2} \sin \omega t \quad (8)$$

Mode 4 is the last stage in the operation period and after this the cycle of operation is repeated.

4 Design of resonant circuit parameters

The proposed resonant circuit ($L_s C_p$) connected to the equivalent circuit of the ozone chamber is shown in Fig. 4. In fact, it behaves similar to a parallel-loaded resonant (PLR) circuit. If the voltage gain is sufficiently high (to ensure the production of microdischarges), the transformer can be omitted. The maximum voltage gain of the PLR circuit is given by

$$A_{vm} = \left| \frac{v_g(j\omega)}{v_{in}(j\omega)} \right| = \frac{Q_p}{\sqrt{1 - 1/4Q_p^2}} \quad (9)$$

where Q_p is the loaded quality factor and is given by

$$Q_p = \frac{R_g}{\omega_p L_s} = \omega_p C_t R_g \quad (10)$$

In (10), ω_p and C_t are given by

$$\omega_p = \frac{1}{\sqrt{L_s C_t}} \quad (11)$$

$$C_t = C_p + C_g \quad (12)$$

The objective of the design is to calculate the values of the $L_s C_p$ circuit to achieve high voltage across the ozone chamber near the vicinity of the given resonant frequency. The voltage, current and losses are maximum at the resonant frequency. At this operating point, Q_p is high and $A_{vm} \approx Q_p$. The average power supplied to the ozone chamber is calculated by the power dissipated in R_g and is

given as

$$P_{avg} = \frac{v_{g,rms}^2}{R_g} \quad (13)$$

The average power is supplied at resonant frequency, where the power factor is unity. The voltage gain is given by

$$A_{vm} = \frac{v_{g,rms}}{v_{in,rms}} \quad (14)$$

Since the inverter output voltage waveform v_{AB} (Fig. 11) looks like a quasi-square wave, for simplicity, an approximation to a square wave is made. Hence, the root-mean-square value of the inverter output waveform can be formulated as

$$v_{in,rms} = \frac{\sqrt{2}}{\pi} V_{DC} \quad (15)$$

Combining (13)–(15), it follows that

$$A_{vm} = \frac{\pi\sqrt{P_{avg}R_g}}{\sqrt{2}V_{DC}} \quad (16)$$

The resonant circuit inductance (L_s) and capacitance (C_p) can be calculated by combining (10) and (16) yields

$$L_s = \frac{\sqrt{2}V_{DC}}{\pi\omega_p} \sqrt{\frac{R_g}{P_{avg}}} \quad (17)$$

$$C_p = \frac{\pi}{\sqrt{2}\omega_p V_{DC}} \sqrt{\frac{P_{avg}}{R_g}} - C_g \quad (18)$$

The values of L_s and C_p are calculated to deliver average power of 8 W. The values of L_s and C_p calculated from (17) and (18) are 3.63 mH and 636.6 pF, respectively. The ETD-44 3C90 ferrite core is used to implement the designed value of the inductor. The designed value of C_p is implemented using series–parallel connections of 1500 and 1000 pF medium voltage (700 V_{rms}) capacitors. Using the calculated values of L_s , C_p and chamber parameters from Section 2, the Q_p is calculated to be 124.8. The frequency response of the ‘LC’ resonant circuit for various Q_p is shown in Fig. 7. As can be seen that the PLR circuit exhibits high-voltage gain for higher values of Q_p . The voltage gain at selected operating frequency (96.3 kHz) is 40.

The state-space equations of the $L_s C_p$ circuit and ozone chamber parameters are developed to understand the relation between input voltage (v_{AB}), the current (i_{in}) and the chamber voltage (v_g). The two state equations describing the time behaviour of the circuit in Fig. 4 can be written as

$$\frac{di_{in}}{dt} = \frac{1}{L_s} v_{AB} - \frac{1}{L_s} v_g \quad (19)$$

$$\frac{dv_g}{dt} = \frac{1}{C_p} i_{in} - \frac{1}{C_p C_g R_g} v_g \quad (20)$$

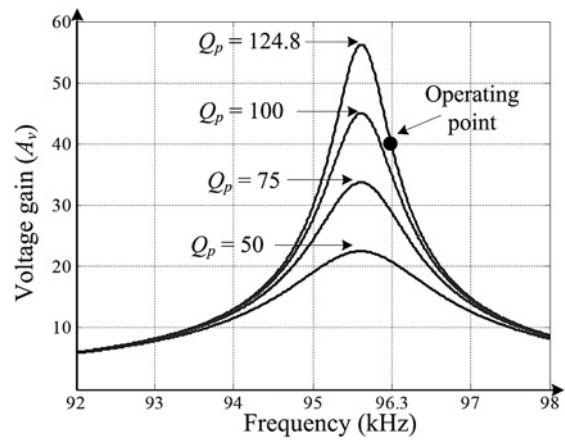


Fig. 7 Voltage gain frequency response of $L_s C_p$ resonant circuit

The state-space equation is derived as

$$\frac{d}{dt} \begin{bmatrix} i_{in} \\ v_g \end{bmatrix} = \begin{bmatrix} 0 & -\frac{1}{L_s} \\ \frac{1}{C_p} & -\frac{1}{C_p C_g R_g} \end{bmatrix} \begin{bmatrix} i_{in} \\ v_g \end{bmatrix} + \begin{bmatrix} \frac{1}{L_s} \\ 0 \end{bmatrix} \cdot [v_{in}] \quad (21)$$

Using the calculated values of resonant circuit and chamber parameters, the MATLAB/Simulink model is developed utilising (21). The resonant circuit input waveforms voltage, the input current and chamber voltage are plotted as shown in the Fig. 8. It is noted that the converter operates above the resonant frequency of resonant circuit; the current i_{in} lags the v_{AB} .

The resonant frequency depends on the values of L_s and C_p , in addition to the chamber parameters. The effect of varying the combinational values of $L_s C_p$ within $\pm 5\%$ of their designed values is shown in Fig. 9. As can be seen, while f_r varies because of the variation in the components, the amplitude of the resonant peak remains constant. To ensure that ZVS is achieved, the operational frequency must be adjusted to be (slightly) higher than f_r . To resolve this issue, it is necessary to include a closed-loop feedback control to the system to ensure that the inverter’s operating point is always located (slightly) above f_r at or near the designated the gain value. If there is a deviation in the operating point,

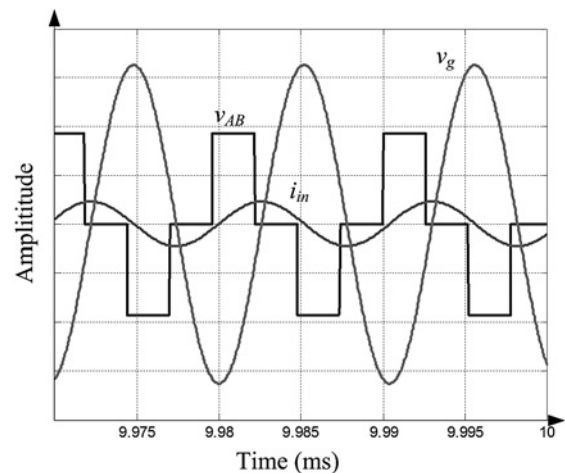


Fig. 8 Simulated input voltage v_{AB} , input current i_1 and output voltage v_g

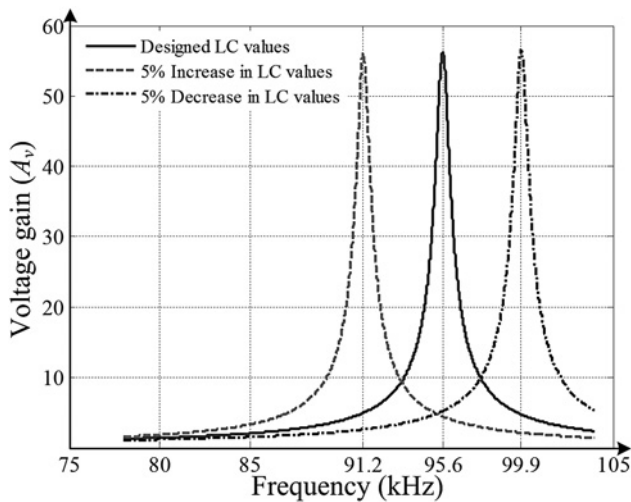


Fig. 9 Voltage gain against frequency with $L_s C_p$ parameters variation

Table 1 Parameters of the prototype ozone generator

Parameter	Symbol	Value	Unit
series inductance	L_s	3.63	mH
parallel capacitance	C_p	636.6	pF
chamber capacitance	C_g	136.6	pF
chamber resistance	R_g	270	k Ω

the control circuit is expected to track the change and adjusts the switching frequency of the inverter accordingly. The design and implementation of such closed-loop control circuit is quite involved, and has been described elsewhere [25]. The proposed ozone generator parameters are summarised in Table 1.

5 Results and discussion

To prove the viability of the proposed method, the ozone generator prototype has been implemented and tested. Moreover, the simulation is carried out using MATLAB/simulink to check the validity of the designed parameters. The chamber voltage is controlled by the input DC power supply of the inverter, whereas the switching frequency (96.3 kHz) of the inverter is kept constant by the gate drive circuit. Fig. 10 shows the gating signal of the switches, together with the output current of the inverter. As can be seen, the switches turn on at zero current. Hence, zero turn on current switching is achieved. However, the turn-off losses are still present. When either of the switches M_1 or M_2 is ON (intervals t_0-t_1 and t_2-t_3), the input voltage (v_{AB}) to the resonant circuit is $+V_{dc}/2$ or $-V_{dc}/2$, respectively, as can be seen in Fig. 11. When both switches are OFF, the current is diverted into snubber capacitors to charge them; the resonant circuit input voltage will swing towards opposite rail (intervals t_1-t_2 and t_3-t_4). As can be observed, the experimental oscillogram match with the theoretical waveforms shown in Fig. 5.

Fig. 12 depicts the voltage across the chamber as a function of the inverter input voltage. The simulation shows that the chamber voltage varies almost linearly with the input of the inverter. However, experimentally there is a slight difference; the equivalent series resistance of L_s and C_p are

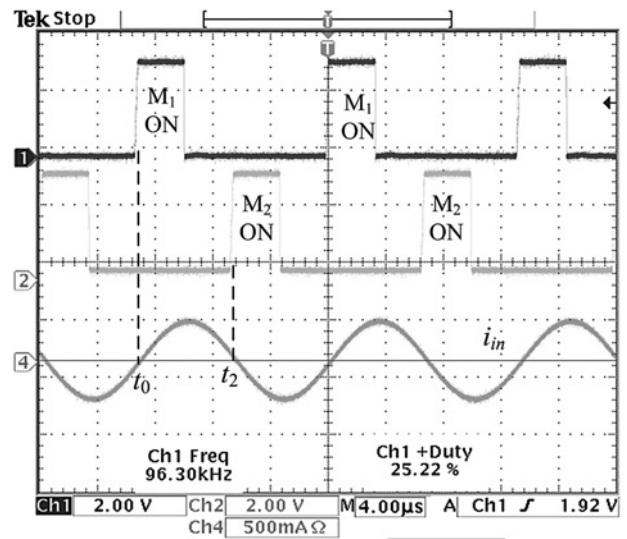


Fig. 10 Top: Half-bridge gating signals; bottom: resonant circuit input current

not included in the simulation model, which results in a voltage drop in the output values. Furthermore, for the experimental results, the increase in the chamber voltage is not linear beyond 3.12 kV_{p-p} because of the fact that saturation occurs in the chamber. This phenomenon is consistent with the interpretation reported by other researchers [7, 26].

A simulation and experimental snapshot of the chamber voltage and current waveforms are illustrated in Fig. 13. As predicted, the voltage and current waveforms are sinusoidal at resonance. The current leads the voltage because the ozone chamber behaves as a capacitive load. The presence of microdischarges can be observed from the spikes that ride on the experimental current waveform. By increasing the voltage, the amplitude and duration of the microdischarges increase during both cycles of the current; this increases the ozone production. The ‘LC’ resonant circuit is capable of generating a sinusoidal output voltage of 3.2 kV_{p-p}, which is adequate to initiate microdischarge and sustain ozone formation in the chamber.

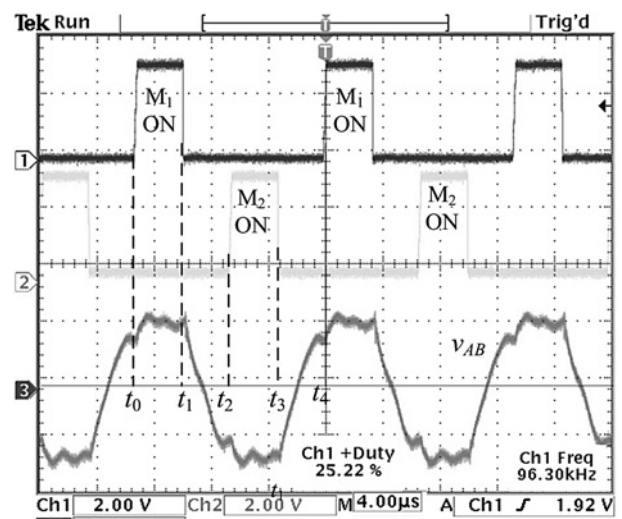


Fig. 11 Top: Half-bridge gating signals; bottom: resonant circuit input voltage

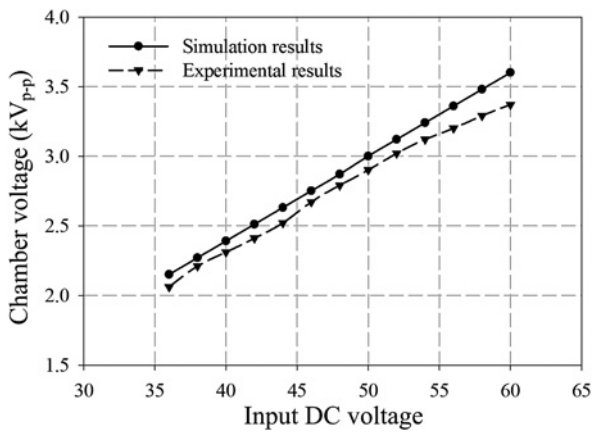


Fig. 12 Voltage gain frequency response of LC resonant circuit

The ozone quantity can be quantified in two ways: by its concentration (g/m^3) or by its efficacy (g/kWh). The latter is more recognisable as the figure of merit for ozone generation. In this work, the concentration is measured (in the scale of $\mu\text{g/m}^3$) using the InDevR 2B Technologies, UV 106 ozone monitor. The discharge gap is fed with 95% oxygen at a flow of 1.0 l/min. Fig. 14 shows the variation of the ozone concentration with the chamber voltage. Two separate experiments are carried out to obtain high voltage across the chamber at different frequencies. The first one is using the designed values L_s , C_p which gives resonant frequency of 95.8 kHz. Secondly, by varying the values of L_s and C_p , the resonant frequency is changed to 33 kHz. Two operating frequencies are compared: 96.3 kHz (Case 1) and 33.4 kHz (Case 2) [16]. For Case 1, the initiation voltage starts at 2.1 kV_{p-p} , which is slightly lower than for Case 2 (2.3 kV_{p-p}). Furthermore, the maximum ozone concentration (9.5 g/m^3) for Case 1 occurs at a lower voltage, that is, at 3.2 kV_{p-p} . On the other hand, the maximum ozone concentration achieved for Case 2 is 7.2 g/m^3 . This value is recorded at the chamber voltage of 3.7 kV_{p-p} . From the results, it can be deduced that the performance of the ozone generator (both in terms of lower initiation voltage and higher yield), is superior when operated at higher frequency. These observations are consistent with the findings from other researchers, for example [6, 27].

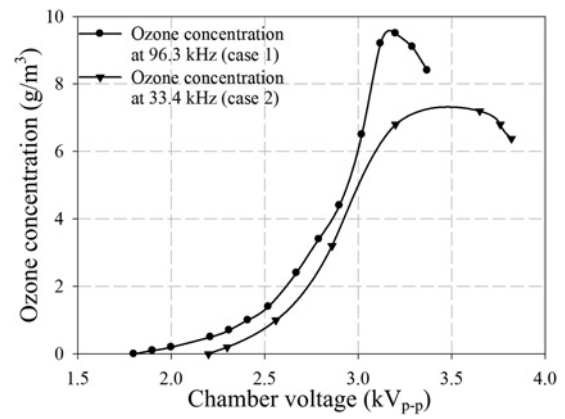


Fig. 14 Ozone concentration against chamber voltage

Fig. 15 illustrates the ozone efficacy. This is a measure that quantifies the production of ozone with respect to the power drawn by the chamber. The efficacy, η (in g/kWh), is calculated by the following equation

$$\eta = \frac{[\text{O}_3] \cdot f \cdot 60}{P} \quad (22)$$

where $[\text{O}_3]$ is the ozone concentration (g/m^3), f is the oxygen flow rate (l/min) and P is the chamber consumed power (W).

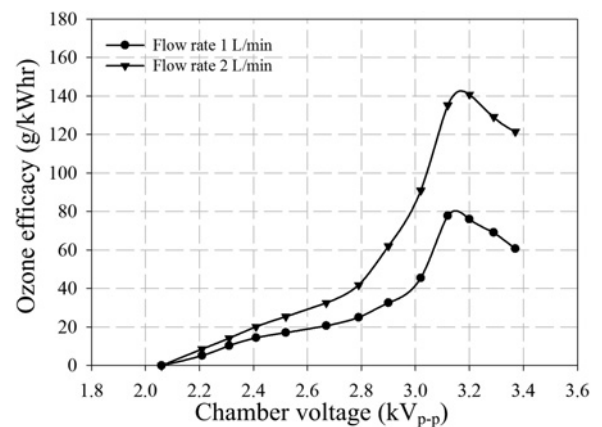
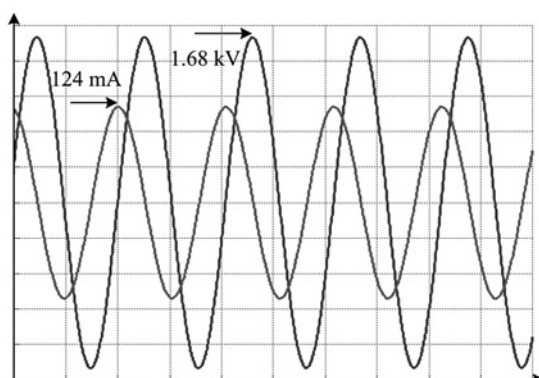
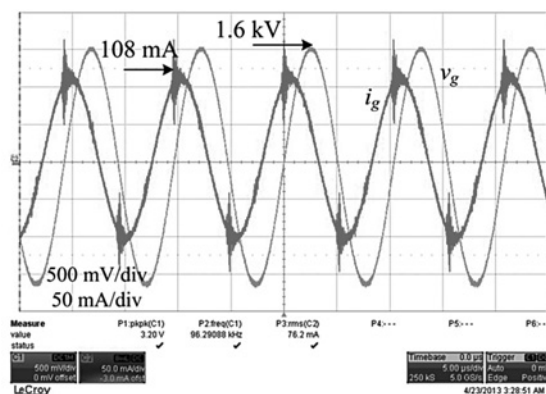


Fig. 15 Ozone efficacy against chamber voltage



Simulation



Experimental

Fig. 13 Chamber voltage and current waveforms at inverter input voltage of 56 V

Note: high-voltage probe scale 1000:1

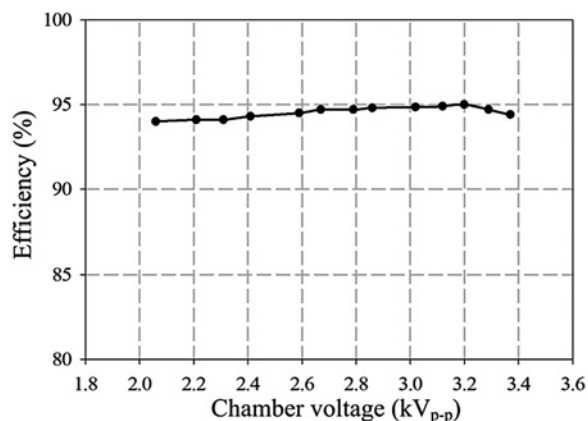


Fig. 16 Efficiency of power converter against chamber voltage

The maximum ozone efficacy that can be achieved by the proposed generator is 140 g/kWh at a flow rate of 2 l/min. Compared with other small-scale ozone generation systems, the achieved ozone production can be considered high [21, 28]. This amount of ozone is large enough for domestic drinking water disinfection and for cleaning of residual pesticide on vegetables and fruits for household applications [29].

The efficiency of the power converter as a function of chamber voltage is shown in Fig. 16. The input power measurement is carried out by power analyser (Voltech PM6000), which is placed between the DC power supply and inverter. On the output side, because of the high-voltage limitation of power analyser, the chamber voltage is measured using an oscilloscope with high-voltage

isolated probes. The power supplied to the chamber is calculated by the power dissipated by equivalent resistance R_g of the chamber [22]. Thus, the difference between the input power and the power supplied to the chamber can be considered as the power converter and resonance losses. Using this measurement approach, the maximum resonant converter efficiency is 95% at the chamber voltage of 3.2 kV_{p-p}, which is significantly higher than transformer-based power supplies [6, 9, 12]. As noted earlier, beyond 3.2 kV_{p-p}, the increase in chamber voltage will not increase the ozone yield further, because of the saturation that takes place in the chamber [7]. Furthermore, the power losses in the 'LC' resonant circuit also contribute to the decrease in the efficiency, particularly near the maximum voltage region.

To simplify the discussion, Table 2 summarises the performance of the proposed 'LC' resonant converter in comparison with the previous transformer-based converters for ozone generation. The proposed converter requires two switches and 'LC' resonant circuit to create high voltage across the chamber. It can be realised using low cost, standard materials. Furthermore, since the transformer is absent, its efficiency is higher compared with the transformer-based power supplies and requires small footprint. In previous works, a step-up transformer and inductors (placed at primary/secondary) is used [1, 2, 10]. Owing to the leakage inductance of the transformer, protection circuitry is required to curtail the inductive spikes. As a result, the cost and size of transformer-based converter is increased. Although the converter in [7–9] produces higher ozone, its chamber is much more costly: its electrodes are covered by thin film such as gold or platinum. For the PT-based converter [13–15], its efficiency is approximately equal to the proposed converter. However,

Table 2 Proposed resonant converter comparison with the previous work

Reference	Topology	Ozone chamber configuration	Input DC voltage, V	Frequency, kHz	Maximum chamber voltage, kV _{p-p}	Maximum ozone efficacy, g/kWh	Efficiency, %
[6]	full-bridge resonant inverter	shape: circular electrodes: stainless steel dielectric: borosilicate glass	310	57.5	3.44	20.0	87
[7–9]	push–pull resonant inverter	shape: circular glass tube filled with discharge gas argon electrodes: stainless steel covered by film of noble metal, that is, gold/platinum dielectric: alumina ceramic	50	5.0	7	194	78
[10–12]	single-switch resonant inverter	shape: circular glass tube filled with discharge gas argon electrodes: stainless steel covered by film of noble metal, that is, gold/platinum dielectric: alumina ceramic	403	15.0	2.8	6.0	50
[13–15]	class D resonant inverter with PT	shape: circular glass tube electrodes: stainless steel dielectric: alumina ceramic	175	40.6	5.7	30.0	95
this work	half-bridge based on LC resonant circuit	shape: rectangular electrodes: aluminium mesh and copper plate dielectric: muscovite mica	60	96.3	3.6	140	95

the high-power PTs are costly and not readily available in the market at a reasonable cost.

6 Conclusions

In this paper, an 'LC'-based half-bridge resonant converter has been investigated to supply an ozone chamber at high frequency. The use of the high-frequency resonant converter permits an increase in the power density of the chamber electrode surface, while decreasing the applied voltage required. To verify the theory, ozone production at two operating frequencies is compared. Thus, an increased ozone production is observed for a given electrode surface area. Conversely, the use of the 'LC' circuit allows us to generate high voltage across the chamber and the use of transformer is omitted. The advantage of the proposed power converter is its low component count and high efficiency. The design and implementation of the power converter prototype have been described.

7 References

- 1 Samaranayake, W.J.M., Namihira, E., Katsuki, S., *et al.*: 'Pulsed power production of ozone using nonthermal gas discharges', *IEEE Electr. Insul. Mag.*, 2001, **17**, (4), pp. 17–25
- 2 Kogelschatz, U.: 'Dielectric-barrier discharges: their history, discharge physics, and industrial applications', *Plasma Chem. Plasma Process.*, 2003, **23**, (1), pp. 1–46
- 3 Dimitrou, M.A.: 'Design guidance manual for ozone systems' (IOA Pan American Committee, Norwalk, CT, 1990)
- 4 Buntat, Z., Smith, I.R., Razali, N.A.M.: 'Ozone generation using atmospheric pressure glow discharge in air', *J. Phys. D, Appl. Phys.*, 2009, **42**, (23), pp. 1–5
- 5 Koudriavtsev, O., Shengpei, W., Konishi, Y., Nakaoka, M.: 'A novel pulse-density-modulated high-frequency inverter for silent-discharge-type ozonizer', *IEEE Trans. Ind. Appl.*, 2002, **38**, (2), pp. 369–378
- 6 Kinnarees, V., Hothongkham, P.: 'Circuit analysis and modeling of a phase-shifted pulsewidth modulation full-bridge-inverter-fed ozone generator with constant applied electrode voltage', *IEEE Trans. Power Electron.*, 2010, **25**, (7), pp. 1739–1752
- 7 Alonso, J.M., Garcia, J., Calleja, A.J., Ribas, J., Cardesin, J.: 'Analysis, design, and experimentation of a high-voltage power supply for ozone generation based on current-fed parallel-resonant push-pull inverter', *IEEE Trans. Ind. Appl.*, 2005, **41**, (5), pp. 1364–1372
- 8 Alonso, J.M., Ordiz, C., Gacio, D., Ribas, J., Calleja, A.J.: 'Closed-loop regulated power supply for ozone generation based on buck converter and current-fed push-pull resonant inverter'. Thirteenth European Conf. Power Electronics and Applications, 2009, pp. 1–10
- 9 Ordiz, C., Alonso, J.M.J., Costa, M.A.D., Ribas, J., Calleja, A.J.: 'Development of a high-voltage closed-loop power supply for ozone generation'. Twenty-Third Annual IEEE Applied Power Electronics Conf. and Exposition, 2008, pp. 1861–1867
- 10 Alonso, J.M., Calleja, A.J., Ribas, J., *et al.*: 'Low-power high-voltage universal-input inverter for ozone generation'. Eighth IEEE Int. Power Electronics Congress, 2002, pp. 153–159
- 11 Alonso, J.M., Calleja, A.J., Ribas, J., Valdes, M., Losada, J.: 'Analysis and design of a low-power high-voltage high-frequency power supply for ozone generation'. Thirty-Sixth IAS Annual Meeting. Conf. Record of Industry Applications Conf., 2001, pp. 2525–2532
- 12 Alonso, J.M., Cardesin, J., Corominas, E.L., Rico-Secades, M., Garcia, J.: 'Low-power high-voltage high-frequency power supply for ozone generation', *IEEE Trans. Ind. Appl.*, 2004, **40**, (2), pp. 414–421
- 13 Alonso, J.M., Ordiz, C., Dalla Costa, M.A., Ribas, J., Cardesin, J.: 'High-voltage power supply for ozone generation based on piezoelectric transformer', *IEEE Trans. Ind. Appl.*, 2009, **45**, (4), pp. 1513–1523
- 14 Alonso, J.M., Ordiz, C., Costa, M.A.D., Ribas, J., Cardesin, J.: 'High voltage power supply for ozone generation based on piezoelectric transformer'. Forty-Second IAS Annual Meeting Industry Applications Conf., 2007, pp. 1901–1908
- 15 Alonso, J.M., Ordiz, C., Dalla Costa, M.A.: 'A novel control method for piezoelectric-transformer based power supplies assuring zero-voltage-switching operation', *IEEE Trans. Ind. Electron.*, 2008, **55**, (3), pp. 1085–1089
- 16 Amjad, M., Salam, Z., Facta, M., Mekhilef, S.: 'Analysis and implementation of transformerless LCL resonant power supply for ozone generation', *IEEE Trans. Power Electron.*, 2013, **28**, (2), pp. 650–660
- 17 Facta, M., Salam, Z., Buntat, Z., Yuniarto, A.: 'Silent discharge ozonizer for colour removal of treated palm oil mill effluent using a simple high frequency resonant power converter'. IEEE Int. Conf. Power and Energy, 2010, pp. 39–44
- 18 Facta, M., Salam, Z., Jusoh, A., Bin Buntat, Z.: 'Improvement in ozone generation with low voltage high frequency power converters'. IEEE Second Int. Power and Energy Conf., 2008, pp. 1446–1450
- 19 Kazimierczuk, M.K., Darius, C.: 'Resonant power converter' (John Wiley and Sons, 1995)
- 20 Langlais, B., Reckhow, D., Brink, D.: 'Ozone in water treatment: application and engineering: cooperative research report' (Lewis Publishers, Chelsea, Michigan, 1991)
- 21 Haverkamp, R.G., Miller, B.B., Free, K.W.: 'Ozone production in a high frequency dielectric barrier discharge generator', *Ozone, Sci. Eng.*, 2002, **24**, pp. 321–328
- 22 Alonso, J.M., Valdés, M., Calleja, A.J., Ribas, J., Losada, J.: 'High frequency testing and modeling of silent discharge ozone generators', *Ozone, Sci. Eng.*, 2003, **25**, (5), pp. 363–376
- 23 Amjad, M., Salam, Z., Facta, M., Ishaque, K.: 'A simple and effective method to estimate the model parameters of dielectric barrier discharge ozone chamber', *IEEE Trans. Instrum. Meas.*, 2012, **61**, (6), pp. 1676–1683
- 24 Sekiya, H., Sagawa, N., Kazimierczuk, M.K.: 'Analysis of class DE amplifier with nonlinear shunt capacitances at any grading coefficient for high Q and 25% duty ratio', *IEEE Trans. Power Electron.*, 2010, **25**, (4), pp. 924–932
- 25 Amjad, M., Salam, Z.: 'Analysis, design, and implementation of multiple parallel ozone chambers for high flow rate', *IEEE Trans. Ind. Electron.*, 2014, **61**, pp. 753–765
- 26 Alonso, J.M., Garcia, J., Calleja, A.J., Ribas, J., Cardesin, J.: 'Analysis, design and experimentation of a high voltage power supply for ozone generation based on the current-fed parallel-resonant push-pull inverter'. Industry Applications Conf., 2004, pp. 2687–2693
- 27 Hothongkham, P., Kinnarees, V.: 'Constant voltage control of high voltage high frequency power supply for ozone quantity adjustment', *IEEE Int. Symp. Circuits Syst.*, 2009, pp. 1977–1980
- 28 Takayama, M., Ebihara, K., Stryczewska, H., *et al.*: 'Ozone generation by dielectric barrier discharge for soil sterilization', *Thin Solid Films*, 2006, **506**–**507**, pp. 396–399
- 29 Wu, J.G., Luan, T.G., Lan, C.Y., Lo, W.H., Chan, G.Y.S.: 'Efficacy evaluation of low-concentration of ozonated water in removal of residual diazinon, parathion, methyl-parathion and cypermethrin on vegetable', *J. Food Eng.*, 2007, **79**, (3), pp. 803–809